ARCHIVIO ISTITUZIONALE DELLA RICERCA

Alma Mater Studiorum Università di Bologna
Archivio istituzionale della ricerca

Control of the torque and rotor power in a five-phase wound-rotor induction motor drive for rotary assembly platforms

This is the final peer-reviewed author's accepted manuscript (postprint) of the following publication:

Published Version:
Rizzoli, G., Mengoni, M., Sala, G., Zarri, L., Tani, A. (2020). Control of the torque and rotor power in a five-phase wound-rotor induction motor drive for rotary assembly platforms. Institute of Electrical and Electronics Engineers Inc. [10.1109/ICEM49940.2020.9270773].

Availability:
This version is available at: https://hdl.handle.net/11585/787879 since: 2025-01-23

Published:

DOI: http://doi.org/10.1109/ICEM49940.2020.9270773

Terms of use:

Some rights reserved. The terms and conditions for the reuse of this version of the manuscript are specified in the publishing policy. For all terms of use and more information see the publisher's website.

This item was downloaded from IRIS Università di Bologna (https://cris.unibo.it/).
When citing, please refer to the published version.

(Article begins on next page)

07 December 2025

Control of the Torque and Rotor Power in a Five-Phase Wound-Rotor Induction Motor Drive for Rotary Assembly Platforms

G. Rizzoli, M. Mengoni, G. Sala, L. Zarri, A. Tani

Abstract - **This paper illustrates the control system of a five-phase wound-rotor induction machine that can be used in applications where, besides the torque generation, a certain amount of active power must be transferred to loads collocated on the rotor frame. This requirement is common in rotary assembly platforms, bottle filling and capping systems, that embed electric actuators, sensors and process controllers on a rotating disk. The use of a five-phase machine avoids the slip-ring contacts to feed the rotor load. However, the choice of the set-point values for the motor currents involves magnetic, electric and thermal constraints. The paper illustrates a methodology of analysis, and develops a technique to deliver power to the rotor loads through the third-order spatial component of the magnetic field, while keeping the motor torque under control and reducing the rotor current as much as possible to minimize the rotor Joule losses. The experimental tests on a scaled prototype demonstrate the practical potential of the machine.**

Index Terms - **Variable speed drives, Induction motors, Inductive power transmission.**

I. Introduction

Bottle filling and capping systems are often based on an assembly rotary table, namely a rotating disk, moved by a gear-motor, which carries the objects to be machined. Some machining stations, placed on the stationary frame around the table, process the objects sequentially. In modern automatic machineries, some actuators used for additional positioning or measurements are located on the rotating disk. Sliding electrical contacts are usually adopted to feed these rotor loads, although they may require demanding preventive replacement due to continuous wear [1]. Instead of slip-rings, the use of rotary transformers enables the contactless transfer of power to the loads on the moving platform [2]-[3].

However, the rotary transformer can be integrated in the gear-motor that drives the platform. Although solutions with three-phase and multi-phase wound-rotor induction machines have been developed [4]-[5], those based on multiphase machines ensure a better quality of the magnetic torque. While the main contribution to the torque is given by the fundamental spatial component of the air-gap magnetic field, the third-order spatial harmonic can be used to transfer power to the rotor loads. This is possible because, in multiphase machines, not only the fundamental spatial component of the air-gap flux can be controlled, but also some higher order harmonics [6], depending on the number of phases.

G. Rizzoli, M. Mengoni, G. Sala, L. Zarri, A. Tani are with the Department of Electrical and Information Engineering "G. Marconi", University of Bologna, Bologna, Italy (e-mails:gabriele.rizzoli@unibo.it, michele.mengoni@unibo.it, g.sala@unibo.it, luca.zarri2@unibo.it, angelo.tani@unibo.it).

Suitable inverter modulation strategies for multiphase inverters, which allow controlling the field harmonics according to the requirements set by the control system, have already been developed [7]. In multiphase drives, these characteristics have been used to develop fault tolerant drives [8], high torque density machines [9], and sensorless control schemes [10].

The present paper improves the control system of the wound-rotor multiphase machine developed for a rotary assembly platform and illustrated in [5]:

- The control system adjusts the reactive power delivered to the rotor in order to reduce the rotor Joule losses.
- A methodology for the choice of the reference currents that satisfy the electromagnetic and mechanical design constraints is illustrated.

Experimental results obtained on a laboratory prototype prove the feasibility of the proposed solution, which allows the decoupled control of motor torque and rotor power.

II. Description of the System

The control system and the structure of the electric drive are shown in Fig. 1. The direct-drive five-phase wound-rotor induction machine is fed by a stator inverter and a rotor inverter, respectively located on the stationary frame and the rotating disk. The rotor inverter operates as a PWM rectifier and keeps the dc voltage E_{RDC} constant to supply the auxiliary rotor loads.

A. Five-Phase Induction Machine Model

The Vector Space Decomposition (VSD) can be used to split the model of the five-phase induction machine into two sets of equations, written in two reference frames d_1-q_1 and d_3-q_3 rotating with electric angular speeds ω_1 and ω_3 respectively in the fundamental subspace and in the third harmonic subspace [6]. Under the assumption of distributed windings and star connected phases, the set of equations of the motor is as follows:

$$\bar{v}_{S1} = R_S\,\bar{i}_{S1} + j\,\omega_1\,\bar{\varphi}_{S1} + \frac{d\bar{\varphi}_{S1}}{dt} \tag{1}$$

$$\bar{v}_{R1} = R_R\,\bar{i}_{R1} + j\,(\omega_1 - \omega_m)\,\bar{\varphi}_{R1} + \frac{d\bar{\varphi}_{R1}}{dt} \tag{2}$$

$$\bar{\varphi}_{S1} = L_{S1}\,\bar{i}_{S1} + M_1\,\bar{i}_{R1} \tag{3}$$

$$\bar{\varphi}_{R1} = M_1\,\bar{i}_{S1} + L_{R1}\,\bar{i}_{R1} \tag{4}$$

$$\bar{v}_{S3} = R_S\,\bar{i}_{S3} + j\,\omega_3\,\bar{\varphi}_{S3} + \frac{d\bar{\varphi}_{S3}}{dt} \tag{5}$$

$$\bar{v}_{R3} = R_R\,\bar{i}_{R3} + j\,(\omega_3 - 3\omega_m)\,\bar{\varphi}_{R3} + \frac{d\bar{\varphi}_{R3}}{dt} \tag{6}$$

$$\bar{\varphi}_{S3} = L_{S3}\,\bar{i}_{S3} + M_3\,\bar{i}_{R3} \tag{7}$$

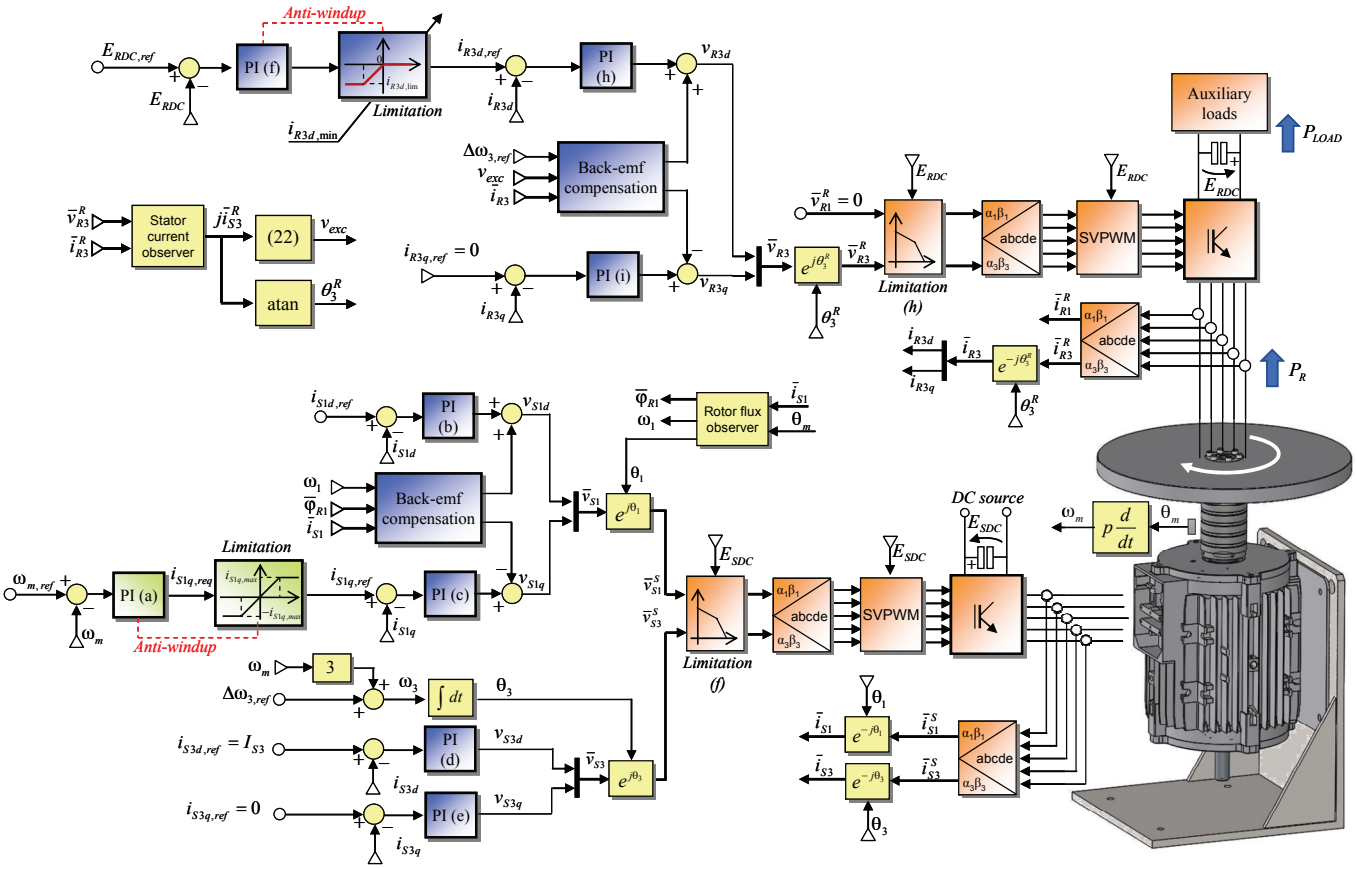

Fig. 1 - Block diagram of the control system and schematics of the five-phase wound-rotor induction motor drive.

$$\bar{\varphi}_{R3} = M_3 \bar{i}_{S3} + L_{R3} \bar{i}_{R3} \tag{8}$$

where $\bar{v}_{Sk}$ and $\bar{v}_{Rk}$ ($k = 1,3$) are the multiple space vectors of the stator and rotor voltages, $\bar{i}_{Sk}$ and $\bar{i}_{Rk}$ ($k = 1,3$) are the multiple space vectors of the stator and rotor currents, $\bar{\varphi}_{Sk}$ and $\bar{\varphi}_{Rk}$ (k=1, 3) are the multiple space vectors of the stator and rotor fluxes, ω_m is the electric speed of the rotor, and L_{Sk}, L_{Rk} and M_k (k = 1, 3) are the self and mutual inductances of the stator and rotor windings.

Each subspace gives a contribution to the total torque, which turns out to be as follows:

$$T = T_1 + T_3 \tag{9}$$

where

$$T_1 = \frac{5}{2} p \left(j \bar{\varphi}_{S1} \cdot \bar{i}_{S1} \right) \tag{10}$$

$$T_3 = \frac{5}{2} p \left(3 j \bar{\varphi}_{S3} \cdot \bar{i}_{S3} \right) \tag{11}$$

being p the number of pole pairs of the motor, and "·" is the scalar product beween vectors.

B. Control of Torque and Rotor Power

The control scheme investigated in this paper is based on the one presented in [5]. However, while in [5] the rotor reactive power Q_R was assumed equal to zero to reduce the power rating of the rotor inverter, here Q_R is controlled to reduce the Joule losses of the rotor windings.

The voltage $\bar{v}_{R1}$ is set to zero, so that (1)-(4) become equal to the equations of a three-phase induction machine with short-circuited rotor windings, and a rotor-field oriented control scheme can be used to adjust the torque contribution T_1. This control system is implemented in a reference frame d_1-q_1 whose d-axis is aligned with the rotor flux $\bar{\varphi}_{R1}$, estimated through the measurement of the rotor position and the integration of the following rotor equation:

$$\tau_{R1} \frac{d\varphi_{R1}}{dt} + \varphi_{R1} = M_1 i_{S1d} \tag{12}$$

where i_{S1d} is the d-component of the stator current vector $\bar{i}_{S1}$, and τ_{R1} is the rotor time constant L_{R1}/R_R.

By combining (3), (4), (10) and (12), the torque contribution T_1 becomes:

$$T_1 = \frac{5}{2} p \frac{M_1}{L_{R1}} \varphi_{R1} i_{S1q} . \tag{13}$$

Therefore, (12) and (13) show that the rotor flux magnitude and torque T_1 can be controlled through the d-q components of the stator current $\bar{i}_{S1}$.

The aim of the rotor control system is to maintain the dc-link voltage constant to feed the electric loads and actuators placed on the rotary table. The rate of change of the electrostatic energy stored in the capacitor C_R can be written as follows:

$$\frac{d}{dt}\left(\frac{1}{2} C_R E_{RDC}^2 \right) = P_R - P_{LOAD} \tag{14}$$

where P_{LOAD} is the power of the rotor loads and P_R is the power of the rotor inverter. When $\bar{v}_{R1}$ is zero, the instantaneous values of the active and reactive rotor powers P_R and Q_R are

$$P_R = -\frac{5}{2}\bar{v}_{R3} \cdot \bar{i}_{R3} \tag{15}$$

$$Q_R = -\frac{5}{2}\bar{v}_{R3} \cdot j\bar{i}_{R3} . \tag{16}$$

Equation (14) shows that adjusting P_R allows controlling the rotor dc-link voltage. To avoid a high-speed exchange of information between the stator and rotor control systems, the following technique can be used to transfer power to the rotor. A rotating space vector $\bar{i}_{S3}^{S}$, with a constant magnitude I_{S3} and a speed-dependent angular frequency ω_3, is generated in the third-order subspace by the stator inverter:

$$\bar{i}_{S3}^{S} = I_{S3} e^{j\omega_3 t} \tag{17}$$

where

$$\omega_3 = 3\omega_m + \Delta\omega_3 . \tag{18}$$

The slip angular frequency $\Delta\omega_3$ is constant, so the current $\bar{i}_{S3}^{S}$, seen by a rotor observer, appears as a rotating vector with a constant frequency independent of the motor speed.

$$\bar{i}_{S3}^{R} = \bar{i}_{S3}^{S} e^{-j3\omega_m t} = I_{S3} e^{j\Delta\omega_3 t} . \tag{19}$$

The superscript "S" or "R" defines variables in reference frames respectively synchronous with the stator or the rotor.

By substituting (8) in (6), the following relationship can be obtained:

$$\begin{aligned} \bar{v}_{R3} = {} & R_R \bar{i}_{R3} + L_{R3}\frac{d\bar{i}_{R3}}{dt} + M_3\frac{d\bar{i}_{S3}}{dt} + \\ & + j(\omega_3 - 3\omega_m)L_{R3}\bar{i}_{R3} + j(\omega_3 - 3\omega_m)M_3\bar{i}_{S3} \end{aligned} \tag{20}$$

If a reference frame d_3-q_3 with the d-axis oriented towards $j\bar{i}_{S3}^{S}$ is used, (20) becomes:

$$\bar{v}_{R3} = R_R \bar{i}_{R3} + L_{R3}\frac{d\bar{i}_{R3}}{dt} + j\,\Delta\omega_3 L_{R3}\bar{i}_{R3} + v_{exc} \tag{21}$$

where v_{exc} is

$$v_{exc} = \Delta\omega_3 M_3 I_{S3} \tag{22}$$

Substituting (22) in (15)-(16) leads to the following equations, which show that the active and reactive powers are functions of the d-q components of the rotor current $\bar{i}_{R3}$.

$$P_R = -\frac{5}{2}\left(R_R\left|\bar{i}_{R3}\right|^2 + v_{exc} i_{R3d}\right) \tag{23}$$

$$Q_R = -\frac{5}{2}\left(\Delta\omega_3 L_{R3}\left|\bar{i}_{R3}\right|^2 - v_{exc} i_{R3q}\right). \tag{24}$$

If the current i_{R3d} is different from zero, a disturbance torque T_3 appears, as can be seen by combining (7), (11) and (22):

$$T_3 = -\frac{15}{2} p \frac{v_{exc} i_{R3d}}{\Delta\omega_3} = -\frac{15}{2} p M_3 I_{S3} i_{R3d} . \tag{25}$$

Since this disturbance is constant at steady state, the control system can easily compensate for it by adjusting T_1.

In conclusion, while the rotor inverter receives power from the rotor windings and keeps the rotor DC-link voltage constant, the stator inverter implements a field-oriented control in the fundamental subspace and generates a current vector $\bar{i}_{S3}$ that rotates at speed $3\omega_m + \Delta\omega_3$ with respect to a stationary observer. Conversely, the rotor reactive power Q_R is a degree of freedom that can be adjusted to reduce the rotor Joule losses, whose expression is as follows:

$$P_{JR3} = \frac{5}{2} R_R\left(i_{R3d}^2 + i_{R3q}^2\right). \tag{26}$$

Minimizing (26) with (23) as a constraint leads to the conclusion that i_{R3q} should be zero, so (24) becomes

$$Q_R = -\frac{5}{2}\Delta\omega_3 L_{R3} i_{R3d}^2 . \tag{27}$$

According to (27), the rotor Joule losses P_{JR3} are at a minimum when the rotor inverter compensates the reactive power of the inductance L_{R3}.

C. Iron Core Saturation

The operating point of the machine must satisfy the constraints due to the rated currents and the saturation of the ferromagnetic materials.

Under the assumptions of linearity and negligible effects of the slot openings, the flux density in the air gap can be approximated as a combination of the fundamental component and the third-order spatial harmonic component [6]:

$$b_0^S(\theta_S, t) = \mathrm{Re}\left[\bar{b}_{01}^{S} e^{-j\theta_S}\right] + \mathrm{Re}\left[\bar{b}_{03}^{S} e^{-j3\theta_S}\right] \tag{28}$$

where θ_s is the stator angular coordinate expressed in electric radians, while $\bar{b}_{01}^{S}$ and $\bar{b}_{03}^{S}$ are vectors representing the sinusoidal distribution of the flux density in the air gap.

$$\bar{b}_{01}^{S} = A_{S1}\bar{i}_{S1}^{S} + A_{R1}\bar{i}_{R1}^{S} \tag{29}$$

$$\bar{b}_{03}^{S} = -\left(A_{S3}\bar{i}_{S3}^{S} + A_{R3}\bar{i}_{R3}^{S}\right). \tag{30}$$

The coefficients A_{S1}, A_{S3}, A_{R1} e A_{R3} are

$$A_{S\rho} = \mu_0 \frac{5 N_S K_{SW\rho}}{2\rho\pi p\delta},\ \rho = (1,3) \tag{31}$$

$$A_{R\rho} = \mu_0 \frac{5 N_R K_{RW\rho}}{2\rho\pi p\delta},\ \rho = (1,3) \quad . \tag{32}$$

where N_S and N_R are respectively the number of conductors in series of a stator and rotor phase, $K_{SW\rho}$ and $K_{RW\rho}$ (ρ = 1, 3) are the harmonic winding factors, and δ is the air gap thickness.

Owing to the asynchronous speeds of the fundamental and third-order field components, the peak value of the flux density in the air-gap, which can be related to the flux density in the teeth and back iron, can be calculated in the worst case as follows:

$$\max\left(b_0^S(\theta_S, t)\right) = \left|\bar{b}_{01}^{S}\right| + \left|\bar{b}_{03}^{S}\right| \tag{33}$$

Equation (33) is valid in any reference system. For the sake of simplicity, the term $\left|\bar{b}_{01}\right|$ is calculated in the reference frame d_1-q_1, while $\left|\bar{b}_{03}\right|$ is calculated in the reference frame d_3-q_3. It can be verified that $\bar{b}_{01}$ can be expressed at steady state as follows:

$$\bar{b}_{01} = A_{S1} i_{S1d} + j\left(A_{S1} - A_{R1}\frac{M_1}{L_{R1}}\right) i_{S1q} \tag{34}$$

where, under the assumption of negligible leakage fluxes, the coefficients of mutual induction M_1 and rotor self-induction L_{R1} are

$$M_1 = \frac{5\mu_0 L\tau N_S N_R K_{SW1} K_{RW1}}{2\pi^2 p\delta} \tag{35}$$

$$L_{R1} = \frac{5\mu_0 L\tau N_R^2 K_{RW1}^2}{2\pi^2 p\delta}. \quad (36)$$

Substituting (32), (35) and (36) in (34) leads to (37).

$$\bar{b}_{01} = A_{S1} i_{S1d}. \quad (37)$$

Hence, $\bar{b}_{01}$ is aligned with the d axis and its magnitude depends only on the magnetizing current i_{S1d}.

Similarly, it is possible to obtain an analytical expression of $\bar{b}_{03}$ in the reference frame d_3-q_3:

$$\bar{b}_{03} = -\left[A_{S3}\left(i_{S3d} + ji_{S3q}\right) + A_{R3}\left(i_{R3d} + ji_{R3q}\right)\right]. \quad (38)$$

At steady state, i_{S3d} is zero, so $i_{S3q} = -I_{S3}$. Furthermore, to minimize the rotor Joule losses, i_{R3q} must be zero. Therefore, (38) becomes:

$$\bar{b}_{03} = -A_{R3} i_{R3d} + jA_{S3} I_{S3}. \quad (39)$$

By using the relationships (37) and (39), the peak value of the total air gap flux density (33) can be expressed as follows:

$$b_{0T,\max} = A_{S1}\left(i_{S1d} + \sqrt{\left(\frac{A_{R3}}{A_{S1}} i_{R3d}\right)^2 + \left(\frac{A_{S3}}{A_{S1}} I_{S3}\right)^2}\right) \quad (40)$$

When the motor operates without involvement of subspace 3, the d component of the stator current cannot exceed the rated value $i_{S1d,rated}$ in order to obtain acceptable values of the iron saturation. If subspace 3 is used to transfer power to the rotor load, the quantity to be compared to $i_{S1d,rated}$ is the expression in brackets in (40), which can be considered as an equivalent magnetizing current.

$$i_{S1d} + \sqrt{\left(\frac{A_{R3}}{A_{S1}} i_{R3d}\right)^2 + \left(\frac{A_{S3}}{A_{S1}} I_{S3}\right)^2} \le i_{S1d,rated} \quad (41)$$

The ratios A_{R3}/A_{S1} and A_{S3}/A_{S1} do not depend on the geometric dimensions of the motor but only on the number of conductors in series and on the winding coefficients.

Besides (41), it is necessary to take into account the constraint resulting from the motor Joule losses. To fully exploit the thermal capability of the stator and rotor windings, the following operating conditions must be imposed:

$$\left|\bar{i}_{S1}^2\right| + \left|\bar{i}_{S3}^2\right| = i_{S,rated}^2 \quad (42)$$

$$\left|\bar{i}_{R1}^2\right| + \left|\bar{i}_{R3}^2\right| = i_{R,rated}^2 \quad (43)$$

Let λ_{S13} be a distribution coefficient defined as follows:

$$\lambda_{S13} = \frac{\left|\bar{i}_{S1}\right|}{\left|\bar{i}_{S3}\right|} \quad (44)$$

Then, introducing (44) in (42) leads to the expressions of $\left|\bar{i}_{S1}\right|$ and $\left|\bar{i}_{S3}\right|$.

$$\left|\bar{i}_{S1}\right| = i_{S,rated}\sqrt{\frac{\lambda_{S13}^2}{1+\lambda_{S13}^2}} \quad (45)$$

$$\left|\bar{i}_{S3}\right| = i_{S,rated}\sqrt{\frac{1}{1+\lambda_{S13}^2}} \quad (46)$$

If i_{S1d} is known, i_{S1q} can be found as follows:

$$i_{S1q} = \sqrt{\left|\bar{i}_{S1}\right|^2 - i_{S1d}^2} \quad (47)$$

Combining (12), (13), (45), (47) leads to an expression for the maximum value of T_1 that is a non-linear function of i_{S1d} and λ_{S13}.

$$T_{1,\max} = \frac{5}{2} p \frac{M_1^2}{L_{R1}} i_{S1d}\sqrt{\frac{\lambda_{S13}^2}{1+\lambda_{S13}^2} i_{S,rated}^2 - i_{S1d}^2}. \quad (48)$$

Furthermore, in conditions of field orientation, the rotor current is

$$\left|\bar{i}_{R1}\right| = \left|i_{R1q}\right| = \frac{M_1}{L_{R1}} i_{S1q}. \quad (49)$$

Replacing (49) in (43) and recalling that i_{R3d} is negative and the drive is controlled so that $i_{R3q} = 0$, one finds:

$$i_{R3d} = -\sqrt{i_{R,rated}^2 - \left(\frac{M_1}{L_{R1}} i_{S1q}\right)^2}. \quad (50)$$

If i_{R3d} is known, it is possible to calculate the maximum transferable power to the rotor loads P_R and the torque disturbance T_3 through (23) and (25).

In conclusion, the choice of λ_{S13} and i_{S1d} leads to a precise value of i_{S1q} to generate the maximum torque. This value, together with $\Delta\omega_3$, univocally determines T_1, T_3, and the power P_R transferred to the rotor loads.

The admissible values of λ_{S13} and i_{S1d} are those that do not violate the constraint (41).

Fig. 2, plotted with the machine parameters in Tab. 1, shows the trend of the main design variables as a function of λ_{S13} when (41) becomes an equality. It can be observed that the magnitude of $\left|\bar{b}_{01}\right|$ and $\left|\bar{b}_{03}\right|$ varies for each value of λ_{S13}, but the total amplitude of the air-gap flux density remains constant in compliance with (41). In addition, as λ_{S13} increases, the torque disturbance T_3 decreases. High values of the ratio T_3/T_1 can jeopardize the performance of the drive. Therefore, it is reasonable that a good decoupling between torque production and rotor energy transfer can occur when T_3/T_1 is lower than 5-10%. However, an increase in λ_{S13} has the negative effect of reducing the rotor power P_R. As can be seen from the figure, this reduction can be compensated by an increase in the angular frequency $\Delta\omega_3$.

III. Control System

The control system of the proposed electric drive, shown in Fig. 1, requires two different control boards, devoted to the stator and rotor inverters, which are independent and do not communicate with one another.

A. Control of the Stator Inverter

Two nested control loops control the speed and torque T_1 of the machine. Speed controller (a) calculates the reference value for the torque producing component of the current, $i_{S1q,ref}$, depending on the speed error. Conversely, the

TABLE I
PARAMETERS OF THE FIVE-PHASE MACHINE

$\omega_{m,rated}$ = 5.2 rad/s (50 rpm)	p = 3
R_S = 1.7 Ω	R_R = 4.8 Ω
L_{S1} = 411 mH	L_{S3} = 68 mH
L_{R1} = 939 mH	L_{R3} = 158 mH
M_1 = 555 mH	M_3 = 53 mH
$i_{S,rated}$ = 4.8 A_{RMS}	$i_{R,rated}$ = 2.1 A_{RMS}
$i_{S1d,rated}$ = 3.5 A	

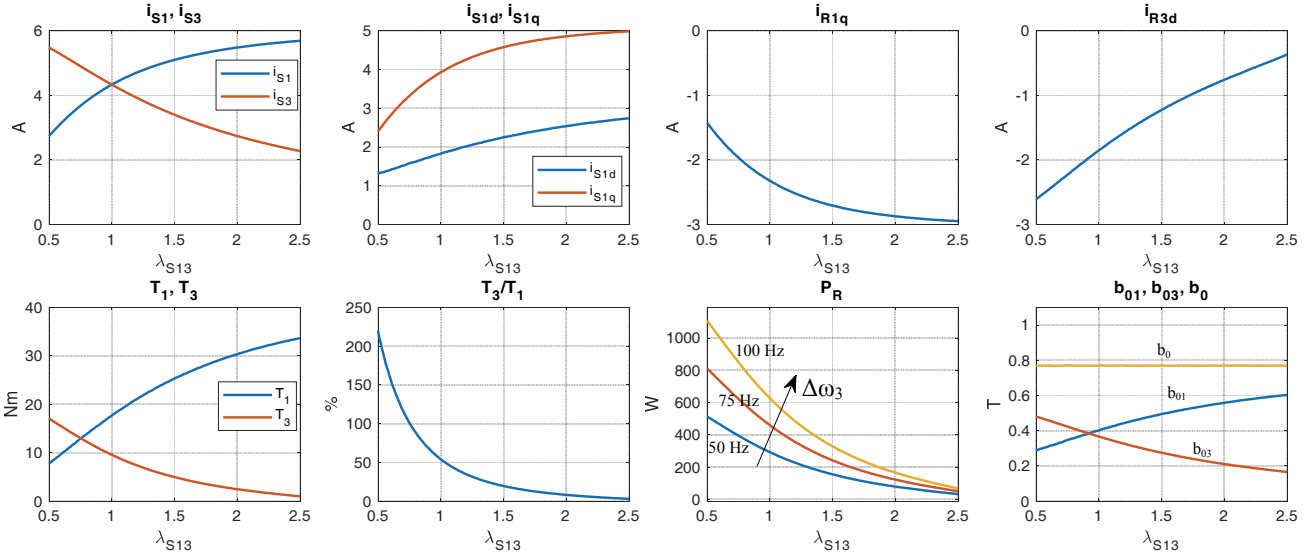

Fig. 2 – Trends of the main electromagnetic and mechanical quantities of the motor as a function of the distribution coefficient λ_{S13}.

magnetizing current $i_{S1d,ref}$ is constant. Two PI regulators, (b) and (c), implemented in the reference frame synchronous with the rotor flux $\overline{\varphi}_{R1}$, are used to track the current references. The reference voltages $v_{S1d,ref}$ and $v_{S1q,ref}$ are compensated for the back-electromotive forces to improve the performance of the current control loops.

A flux observer based on the integration of the rotor equation, expressed in a rotor reference frame, estimates the magnitude, the speed and the phase angle θ_1 of $\overline{\varphi}^S_{R1}$, while an incremental encoder measures the mechanical position of the rotor.

Also, the stator inverter injects the rotating current vector $\bar{i}^S_{S3}$ into the stator windings at angular frequency ω_3, whose value depends on the measured speed according to (18). The integration of ω_3 provides the position θ_3 of the current oriented reference frame d_3-q_3, while two PI regulators, (d) and (e), track the reference currents $i_{S3d,ref}$ and $i_{S3q,ref}$, respectively equal to I_{S3}, and zero.

Finally, the space vector pulse-width modulation is used to generate the desired output voltages $\bar{v}_{S1}$ and $\bar{v}_{S3}$, which are kept in the range of linear modulation by the saturation block (f) [11].

B. *Control of the Rotor Inverter*

As explained in Section II, rotor voltage $\bar{v}_{R1}$ is equal to zero in order to emulate the short-circuited rotor windings in the fundamental subspace.

The control system of the rotor power P_R is implemented in a reference frame whose d axis is aligned with the current vector $j\bar{i}^R_{S3}$. Since the rotor control system cannot measure any stator variable, the estimation of $\bar{i}^R_{S3}$ must be based only on quantities that are available to the rotor control board and can be found by solving (8):

$$\bar{i}^R_{S3} = \frac{\overline{\varphi}^R_{R3} - L_{R3}\,\bar{i}^R_{R3}}{M_3}. \tag{51}$$

where the rotor flux $\overline{\varphi}^R_{R3}$ can be theoretically calculated by integrating (6) rewritten in a rotor reference frame:

$$\overline{\varphi}^R_{R3} = \int \left(\bar{v}^R_{R3} - R_R\,\bar{i}^R_{R3}\right) dt\,. \tag{52}$$

However, a pure integrator cannot be used in practical applications due to the drift caused by measurement offsets and parameter uncertainty, so (52) has been replaced by a low-pass filter, which approximates the ideal behavior of an integrator at angular frequency $\Delta\omega_3$ but has a finite gain at zero frequency [12]:

$$\overline{\varphi}^R_{R3} = \frac{\tau_f}{1+\tau_f s}\left(\bar{v}^R_{R3} - R_R\,\bar{i}^R_{R3}\right). \tag{53}$$

For the selection of the time constant τ_f of the filter, the following condition applies:

$$\frac{1}{\tau_f} < \frac{1}{10}\Delta\omega_3\,. \tag{54}$$

Once current $\bar{i}^R_{S3}$ is available, the active and reactive power can be controlled according to (23) and (24), where the excitation voltage v_{exc} is given by (22).

The reference voltage $\bar{v}_{R3}$ is generated by two PI controllers, (h) and (i), which ensure that the currents i_{R3d} and i_{R3q} are equal to the references $i_{R3d,ref}$ and $i_{R3q,ref}$. The back electromagnetic force components that appear in the rotor voltage equation (21) have been added to the output of the PI controllers to improve the bandwidth of the current control loop. The current reference $i_{R3q,ref}$ is set to zero to reduce the rotor Joule losses, while the current reference $i_{R3d,ref}$ is used by PI (f) to adjust the voltage of the dc bus E_{RDC}.

IV. Experimental Results

A prototype of the proposed electric drive for rotary assembly platforms is shown in Fig. 3. The experimental setup includes a five-phase wound-rotor induction motor, two five-phase inverters based on Infineon F12-25R12KT4G IGBT modules, two floating-point Texas Instruments DSPs, a rotating disk and an active DC load. The electrical parameters of the machine are listed in Table I, and the switching frequency of the converters is 10 kHz. The DC link voltage of the stator inverter is 300 V.

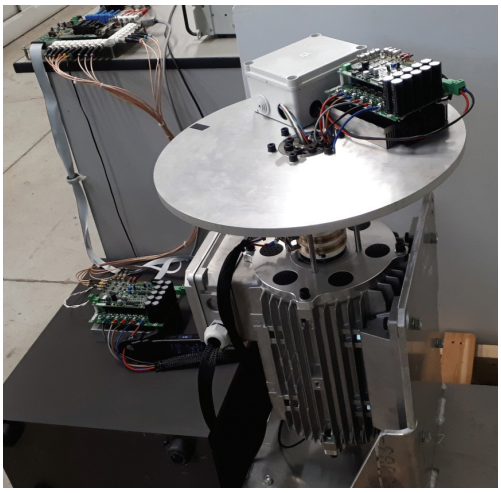

Fig. 3 - Picture of the small-scale drive system for rotary assembly stations.

The results reported in this section have been obtained by imposing λ_{S13} equal to 1.85, i_{S1d} equal to 2.5 A and $\Delta\omega_3$ equal to 100 Hz. In these operating conditions, the maximum torque component T_1 is nearly ± 30 Nm, the maximum power that can be transferred to the rotating loads is 200 W and the theoretical ratio T_3/T_1 is equal to 10.3%.

Fig. 4 shows the space vector decomposition of the stator currents when the speed of the rotor is 70 rpm and the power P_R is 200 W. The phase current i_{Sa} is clearly composed by two sinusoidal harmonics components, the low frequency component is related to T_1, while the high frequency component is related the power transferred to the rotor loads. It can be noted that the loci of vectors $\bar{i}_{S1}^{S}$ and $\bar{i}_{S3}^{S}$ are circular trajectories, which are covered at different angular speeds.

Fig. 5 shows the behavior of the current vector $\bar{i}_{S3}^{S}$ and the estimated excitation voltage $\bar{v}_{exc}^{R}$ (equal to $j\Delta\omega_3 M_3 \bar{i}_{S3}^{R}$) during a speed variation from 0 RPM to 70 RPM while the power P_R is 200 W. The zoomed views of the figure clearly shows that the period of the voltage $\bar{v}_{exc}^{R}$ is 10 ms (100 Hz) and is independent of the mechanical speed of the motor, while the frequency of $\bar{i}_{S3}^{S}$ varies with the mechanical speed

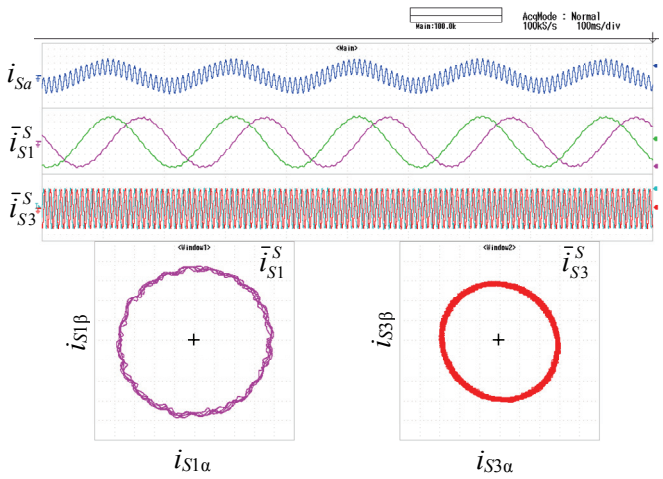

Fig. 4. Space vector decomposition of the stator currents at steady state. Waveforms of the stator phase current i_{Sa} (2.5 A/div), current components $i_{S1\alpha}$ (1 A/div), $i_{S1\beta}$ (1 A/div), $i_{S3\alpha}$ (1 A/div), and $i_{S3\beta}$ (1 A/div).

of the motor according to (19).

Fig. 6 shows the waveforms of the excitation voltage $\bar{v}_{exc}^{R}$, the current $\bar{i}_{R3}^{S}$ and the voltage E_{RDC} during a variation of power P_R from 0 W to 200 W (only the AC component of E_{RDC} is plotted to highlight the transient response). It can be noted that the increase in P_R leads to a reduction in E_{RDC}. The control system of the rotor inverter reacts by increasing the d-component of the current $\bar{i}_{R3}^{S}$. The figure clearly shows that current $\bar{i}_{R3}^{S}$ is in phase opposition with respect to $\bar{v}_{exc}^{R}$, which corresponds to the condition of negative Q_R and i_{R3q} = 0, as discussed in Section II.

The behavior of the drive during a generic working cycle for a rotary assembly station has been emulated. Fig. 7 shows the *d-q* components of current $\bar{i}_{S1}$, the mechanical speed ω_m, the *d-q* components of current $\bar{i}_{R3}$, and the power extracted from the rotor windings P_R. It can be observed that the drive

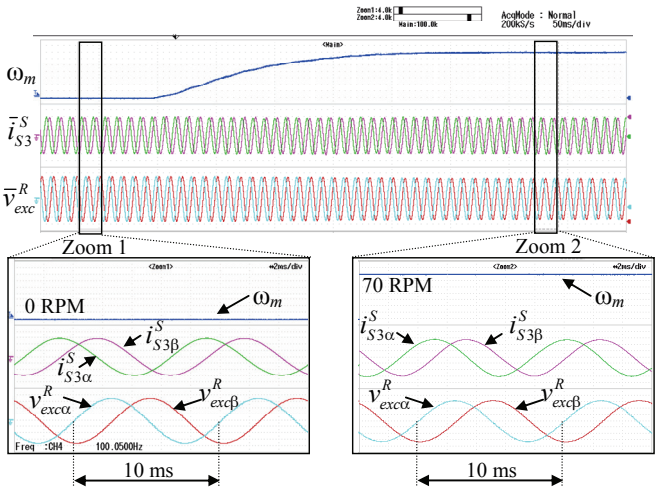

Fig. 5. Behavior of the current vector $\bar{i}_{S3}^{S}$ and of the estimated excitation voltage $\bar{v}_{exc}^{R}$ during a ramp up of the motor from 0 RPM to 70 RPM while the power P_R is equal to 200 W. Waveforms of the mechanical speed ω_m (10 rpm/div), the current components $i_{S3\alpha}$ (1 A/div), $i_{S3\beta}$ (1 A/div), and the voltage components $v_{exc\alpha}$ (25 V/div), and $v_{exc\beta}$ (25 V/div).

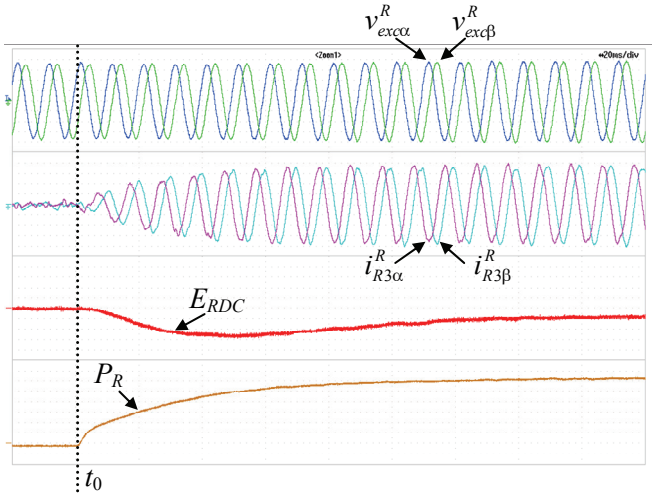

Fig. 6. Behavior of the system in response to a variation of the power P_R. Waveforms of the estimated excitation voltage $v_{exc\alpha}$ and $v_{exc\beta}$ (25 V/div), the rotor current component $i_{R3\alpha}$ and $i_{R3\beta}$ (0.25 A/div), the AC component of the voltage E_{RDC} (1 V/div) and the power P_R (33 W/div)

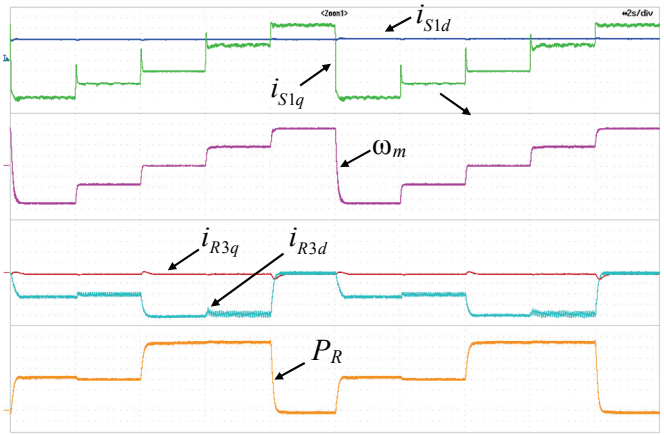

Fig. 7. Emulation of a generic working cycle for rotary assembly stations. Waveforms of the stator current components i_{S1d} and i_{S1q} (1.25 A/div), the mechanical speed ω_m (20 rpm/div), the rotor current components i_{R3d} and i_{R3q} (0.25 A/div), and the power P_R (33 W/div).

can independently control the speed of the rotating disk and the power transferred to the auxiliary actuators, as requested in industrial rotary assembly platforms.

V. Conclusion

This paper illustrates the control system of a five-phase wound-rotor induction machine that can be used in applications that require the generation of the motor torque and the transfer of active power to loads placed on the rotor frame. This type of requirements is common for automatic machineries such as rotary assembly platforms, bottle filling and capping systems.

The definition of the set-point values of the control system is a challenging problem because it involves magnetic, electric and thermal constraints. The paper illustrates the methodology of investigation that has led to the choice of the reference values of the motor currents.

The power delivered to the rotor loads is carried by the third-order spatial component of the magnetic field, and the control system ensures that the rotor current is as low as possible to reduce the rotor Joule losses.

The experimental results have confirmed the feasibility of the proposed electric drive topology and the effectiveness of the decoupled control for torque and transferred power.

VI. References

[1] R. D. Hall and R. P. Roberge, "Carbon brush performance on slip rings," Annual Pulp & Paper Industry Technical Conference, San Antonio, TX, 2010, pp. 1-6.

[2] R. Trevisan and A. Costanzo, "A 1-kW contactless energy transfer system based on a rotary transformer for sealing rollers," *IEEE Trans. Ind. Electron.*, vol. 61, no. 11, pp. 6337-6345, Nov. 2014.

[3] G. Rizzoli, M. Mengoni, L. Zarri and A. Tani, "Voltage Feedback of an LLC Resonant Converter with a Rotary Transformer," Annual Conference of the IEEE Industrial Electronics Society (IECON), Washington, DC, 2018, pp. 1568-1573.

[4] M. Mengoni, G. Rizzoli, L. Zarri, A. Tani, A. Amerise, and G. Serra, "Control of a Three-Phase Wound-Rotor Induction Motor Drive for Automation Applications," in IEEE International Electric Machines & Drives Conference (IEMDC), San Diego, CA, USA, 2019, pp. 1267-1272.

[5] G. Rizzoli, M. Mengoni, A. Tani, G. Serra, L. Zarri, and D. Casadei, "Wireless Power Transfer Using a Five-Phase Wound-Rotor Induction Machine for Speed-Controlled Rotary Platforms," *IEEE Trans. Ind. Electron* (Early Access).

[6] E. Levi, "Advances in converter control and innovative exploitation of additional degrees of freedom for multiphase machines," *IEEE Trans. Ind. Electron.*, Vol. 63, No. 1, pp. 433 - 448, Jan. 2016.

[7] J. Prieto, F. Barrero, M. Duran, S. Marín, M. Perales, "SVM procedure for n-phase vsi with low harmonic distortion in the overmodulation region," IEEE Trans. Ind. Electron., vol. 61, no. 1, pp. 92 -97, Jan. 2014.

[8] N. Bianchi, S. Bolognani, and M. Dai Pre, "Strategies for the Fault-Tolerant Current Control of a Five-Phase Permanent-Magnet Motor," *IEEE Trans. Ind. Appl.*, vol. 43, no. 4, pp. 960-970, July-aug. 2007.

[9] L. Parsa, N. Kim, and H. A. Toliyat, "Field Weakening Operation of High Torque Density Five-Phase Permanent Magnet Motor Drives," in IEEE International Conference on Electric Machines and Drives, San Antonio, TX, 2005, pp. 1507-1512.

[10] F. Barrero and M. J. Duran, "Recent advances in the design, modeling, and control of multiphase machines - part I," *IEEE Trans. Ind. Electron.*, vol. 63, no. 1, pp. 449-458, Jan. 2016.

[11] E. Levi, D. Dujic, M. Jones, G. Grandi, "Analytical determination of dc-bus utilization limits in multiphase VSI supplied AC drives," IEEE Trans. Energy Conv., vol. 23, no. 2, pp. 433-443, June 2008.

[12] J. Holtz, "Sensorless Control of Induction Machines—With or Without Signal Injection?," *IEEE Trans. Ind. Electron.*, vol. 53, no. 1, pp. 7-30, Feb. 2006.

VII. Biographies

Gabriele Rizzoli received the M.Sc and Ph.D. degree in Electrical Engineering, respectively in 2012 and 2016, from the University of Bologna, Bologna, Italy. In 2015 he was a visiting student at Virginiatech (CPES), Blacksburg, Virginia, United States of America. He is currently a research assistant at the Department of Electrical, Electronic and Information Engineering "G. Marconi" of the University of Bologna. His research interests include the design of electrical machines, the development and control of high-efficient power converters for automotive and renewable energy applications.

Michele Mengoni was born in Forlì, Italy. He received the M. Sc. and Ph. D. degrees in Electrical Engineering from the University of Bologna, Bologna, Italy, in 2006 and 2010, respectively. He is currently a Senior Assistant Professor with the Department of Electric, Electronic and Information Engineering "G. Marconi", University of Bologna. His research interests include design, analysis, and control of three phase electric machines, multiphase drives, and ac/ac matrix converters.

Giacomo Sala received the B. Sc. in Power Engineering in 2012, the M. Sc. degree with honors in Electrical Engineering in 2014, and the Ph. D. in Electrical Machines and Drives in 2018 from the University of Bologna, Bologna, Italy. He was a researcher with the Department of Electrical and Electronic Engineering (PEMC group), at The University of Nottingham, until 2019. He joined the Department of Electrical, Electronic and Information Engineering "G. Marconi", University of Bologna in 2019, where he is currently a research assistant. His research interests include design, modeling and control of multiphase machines and drives.

Luca Zarri (M'05-SM'12) received the M. Sc. and Ph.D. degree in Electrical Engineering from the University of Bologna, Bologna, Italy, in 1998 and 2007, respectively. Currently, he is an Associate Professor with the Department of Electrical, Electronic, and Information Engineering "Guglielmo Marconi", University of Bologna. He has authored or coauthored more than 150 scientific papers. His research activity concerns the control of power converters and electric drives. He is a senior member of the IEEE Industry Applications, IEEE Power Electronics and IEEE Industrial Electronics Societies.

Angelo Tani received the M. Sc. degree in Electrical Engineering, with honors, from the University of Bologna, Bologna, Italy, in 1988. Currently he is a Full Professor of power electronics, electrical machines and drives with the Department of Electric, Electronic and Information Engineering, University of Bologna. He has authored more than 180 papers published in technical journals and conference proceedings. His current activities include multiphase and three phase electric drives, diagnostic techniques for electric machines, and active filters.